Available online at www.sciencedirect.com
SCIENCE DIRECT®
Thermochimica Acta 431 (2005) 98–105
thermochimica acta
www.elsevier.com/locate/tca

Transition kinetics of a Ti–Ni alloy examined by temperature-modulated DSC

Akihiko Toda*, Takeshi Arita, Masamichi Hikosaka

Faculty of Integrated Arts and Sciences, Hiroshima University, 1-7-1 Kagamiyama, Higashi-Hiroshima 739-8521, Japan

Received 6 October 2004; received in revised form 5 January 2005; accepted 23 January 2005
Available online 16 February 2005

Abstract

The method of "periodically modulated driving force" with temperature modulated differential scanning calorimetry has been applied to the transition kinetics in Ti_xNi_{100-x}, $x \simeq 50$ at.%. The alloy presents two different types of solid–solid phase transitions. The details of the transition kinetics especially of the ΔT dependence of transition rate has been examined by the present analysis.

Keywords: Modulated driving force; T-M DSC; Ti–Ni; Transition kinetics

1. Introduction

The alloy of Ti–Ni is one of typical shape memory alloys, the behavior of which is closely related with martensitic transformation of the crystals. The transition of this alloy from the parent phase (CsCl-type B2 superlattice) to the martensitic phase (monoclinic B19') on cooling is intervened by an intermediate phase (rhombohedral phase) [1–5]. Both transitions of parent–intermediate phases and intermediate–martensitic phases are first order, but the nature of the transition kinetics is quite different [1–5]. The transition from the parent phase to the intermediate phase is known to be reversible with quite small hysteresis on heating and cooling between those two phases, while the transition to the martensitic phase from the intermediate phase exhibits strong hysteresis, i.e. typical behavior of nucleation controlled growth. Because of those two different types of transition behaviors, the application of "periodically modulated driving force" to this system has a very important meaning by the following reason.

In order to examine transformation kinetics, we have proposed an analyzing method of "periodically modulated driving force" [6] applied by temperature-modulated differential scanning calorimetry (T-M DSC [7–12]). In this method, the driving force of transition, e.g. supercooling in the case of crystallization, is periodically modulated to examine the response of the transition kinetics. The strength of the response is determined by the temperature dependence of transition rate, and hence useful information concerned with the temperature dependence of kinetics can be available by this method. In our previous studies, we have successfully applied this method to the transformation kinetics in polymeric systems, such as crystallization [13], melting [14], solid–solid transition [15] and chemical reaction [16]. The essential point in this method is to examine the frequency dispersion of the response appearing in the effective heat capacity of complex quantity and to determine the characteristic time required for the completion of transition kinetics. A difficult issue arose when the method was applied to polymeric systems with DSC; that is low thermal conductivity in the sample. The examination with different sample thickness showed a systematic variation with thickness, and the thickness must be thin enough for the variation to be small enough to neglect the thermal conductivity. In the present paper, we apply the analyzing method to the transition kinetics of this alloy, which has thermal conductivity ($\simeq 10\,W\,K^{-1}\,m^{-1}$) much better than polymers ($\simeq 0.1$–$0.3\,W\ K^{-1}\,m^{-1}$).

The application of T-M DSC to the martensitic transformation of Ti–Ni alloy has been reported before [17,18], but the analysis was in the stage of qualitative examination of

* Corresponding author. Tel.: +81 82 424 6558; fax: +81 82 424 0757.
E-mail address: atoda@hiroshima-u.ac.jp (A. Toda).

0040-6031/$ – see front matter © 2005 Elsevier B.V. All rights reserved.
doi:10.1016/j.tca.2005.01.049

the transitions with this new technique. The purpose of this paper is to do quantitative examination of the details of those two different types of transition kinetics. In the following, we briefly review the method of "periodically modulated driving force" and report the results of the application to the transition kinetics.

2. Analyzing method of "periodically modulated driving force" with T-M DSC

With T-M DSC, we apply a periodic modulation in temperature with underlying linear heating (cooling) and examine the response in heat flow. The response in heat flow is expressed as a dynamic heat capacity of complex quantity, $\widetilde{\Delta C}\,\mathrm{e}^{-\mathrm{i}\alpha}$, and the relationship between temperature, heat flow, and the dynamic heat capacity is represented as [7–12],

$$T = T_0 + \beta t + \mathrm{Re}[\tilde{T}\,\mathrm{e}^{\mathrm{i}(\omega t+\epsilon)}] \tag{1}$$

$$\dot{Q} = \bar{\dot{Q}} + \mathrm{Re}[\tilde{\dot{Q}}\,\mathrm{e}^{\mathrm{i}(\omega t+\delta)}] \tag{2}$$

$$\widetilde{\Delta C}\,\mathrm{e}^{-\mathrm{i}\alpha} \equiv \widetilde{\Delta C}' - i\widetilde{\Delta C}'' = \frac{\tilde{\dot{Q}}}{\omega\tilde{T}}\,\mathrm{e}^{-\mathrm{i}(\epsilon-\delta-\frac{\pi}{2})} \tag{3}$$

Here, temperature, T, starts from T_0 with underlying linear heating (cooling) of βt and is applied the periodic modulation, $\tilde{T}\,\mathrm{e}^{\mathrm{i}(\omega t+\epsilon)}$, with the amplitude, $\tilde{T}$, angular frequency, $\omega = 2\pi/(\text{period})$, and phase angle, ϵ. Then, heat flow, $\dot{Q}$, is comprised of underlying part, $\bar{\dot{Q}}$, which is the response to the underlying linear heating (cooling) in the case of heating (cooling) run, and the response to the periodic temperature modulation with the amplitude, $\tilde{\dot{Q}}$, and phase angle, δ.

When we apply T-M DSC to transformation kinetics, the dynamic heat capacity includes the response of the kinetics and hence must be treated as an effective heat capacity. If the examined system is made up of small domains and the transition temperature of those domains distributes over a wide temperature range, as is the case of the transition region of Ti–Ni alloy, the steady states of the transition kinetics will be maintained as a whole with the underlying linear heating (cooling) which passes through the transition-temperature region. Therefore, we will be able to see the stationary states responding to the periodic modulation in temperature when the temperature modulation is applied to the underlying linear heating (cooling).

The analyzing method of "periodically modulated driving force" assumes the following rate equation of the kinetics of the untransformed fraction, ϕ, with the rate coefficient, R, dependent on the degree of supercooling (or superheating), $\Delta T \equiv |T_{\mathrm{tr}} - T|$,

$$\frac{\mathrm{d}\phi}{\mathrm{d}t} = -R(\Delta T)\phi \tag{4}$$

With continuous distribution of transition temperatures, T_{tr}, the steady response of the transition kinetics of domains as a whole gives the following approximate expression of the effective heat capacity, $\widetilde{\Delta C}\,\mathrm{e}^{-\mathrm{i}\alpha}$, for power law dependence of R on ΔT with an exponent, y, [6];

$$R \propto \Delta T^{y} \tag{5}$$

$$\widetilde{\Delta C}\,\mathrm{e}^{-\mathrm{i}\alpha} \cong C_{\mathrm{p}} + \frac{-\bar{F}/\beta}{1+\mathrm{i}\omega\tau(\beta)} \tag{6}$$

$$\tau \propto |\beta|^{-x} \tag{7}$$

$$x = \frac{y}{y+1} \tag{8}$$

where C_{p} represents the true heat capacity, $\bar{F}$ the underlying heat flow of transformation kinetics included in $\bar{\dot{Q}}$, and τ the characteristic time which corresponds to the mean time required for the completion of transition of domains and hence becomes shorter with faster underlying heating (cooling) rate because of faster increase in ΔT. The relationship represented by Eqs. (5), (7) and (8) indicates that $R \propto \Delta T^1$ gives $\tau \propto |\beta|^{-0.5}$, and the limit of $y \to \infty$ corresponding to exponential dependence, $\log[R/R_0] \propto \Delta T$, gives $\tau \propto |\beta|^{-1}$. Therefore, by examining the β dependence of the characteristic time τ, the ΔT dependence of transition rate can be available.

This information about the temperature dependence of transition rate is quite valuable when we analyze the transformation kinetics. The dependence is determined by the rate determining process of transition, and hence the quantitative evaluation of the dependence enables us to examine the nature of the transformation. In the case of the first-order phase transition, we can evaluate the nucleation barrier by this method [16]. In principle, the method is applicable to any transition kinetics if the transition region is wide enough to guarantee the steady response of the transition kinetics on linear heating (or cooling); the transitions in Ti–Ni alloy satisfy this requirement.

3. Experimental

A DSC 2920 Module controlled with Thermal Analyst 2200 (TA Instruments) was used for all measurements. Helium gas with a flow rate of 40 mL min^{-1} was purged through the cell. Reference pan was removed to avoid introduction of an uncontrollable parameter of the thermal contact between the reference pan and the base plate [19].

The samples are polycrystalline sheets of $\mathrm{Ti}_x\mathrm{Ni}_{100-x}$, $x \simeq 50$ at.% (TOKIN Corporation). The sample was cold worked to have the thickness change from 215 to 200 μm with a rolling mill at room temperature and then annealed at 120 °C above the transition regions. The samples were directly placed on the sample stage in the DSC cell. The transition behaviors on cooling were examined with the underlying cooling rate of 0.2–3.2 K min^{-1}. Sinusoidal temperature modulation was applied with the modulation period in the range of 10–100 s and the amplitude which satisfies the con-

dition of cooling only, $dT/dt < 0$; the maximum amplitude was set at ± 0.2 K.

In order to determine the effective heat capacity, $\widetilde{\Delta C}\, e^{-i\alpha}$, from the raw data of heat capacity, an appropriate calibration considering the instrumental time constant is required [20]. In the present analysis, the magnitude and the phase angle of the heat capacity have been adjusted for the data outside the transition region. This calibration was justified for the melting of polymer crystals with good thermal conductivity of helium purge gas, and hence will also be applicable to the present sample directly placed on the sample stage.

The condition of steady response of the kinetics were confirmed by plotting two cycles of Lissajous diagram of the modulated heat flow versus modulated sample temperature, which needs to form a closed loop for steady response [21,22].

4. Results and discussion

Fig. 1 represents the dependences of the effective heat capacity on the applied modulation frequency (Fig. 1a and b) and on the underlying cooling rate (Fig. 1c) in the transition regions of Ti–Ni alloy. In Fig. 1, basically three peaks are seen. The peak at around 28 °C represents the transition from the parent phase to the intermediate phase, while the peaks at around 8 and 12 °C represent the one from the intermediate phase to the martensitic phase. Since the peak profile and its position are susceptible to cold work and thermal treatment before the measurement [23], it is most probable that the stress distribution in the sample caused the split of the peak into 8 and 12 °C. Those two peaks at 8 and 12 °C did not show any significant differences in the results of the present analysis, and hence we will concentrate on the behavior of the peak at 12 °C in terms of the transition from the intermediate phase to the martensitic phase in the following discussion.

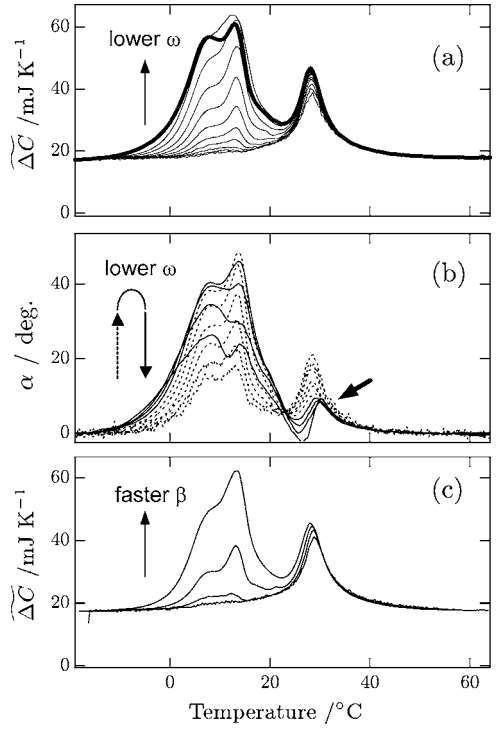

Fig. 1. Effective heat capacity of complex quantity in the transition region of Ti–Ni alloy on cooling. In (a) and (b), the magnitude and the phase angle of the complex heat capacity are shown, respectively, with $-\beta = 1.6\,\mathrm{K\,min^{-1}}$ and the modulation periods of 10, 13, 17, 22, 28, 36, 47, 60, 78 and 100 s. In (a), thick line represents the underlying heat flow which is converted into heat capacity in the plot: $-\dot{\bar{Q}}/\beta$. In (c), the magnitude is shown with fixed modulation period of 78 s at different underlying cooling rates of $-\beta = 0.2$, 0.4, 0.8, 1.6 K min^{-1}.

In Fig. 1, the most distinctive feature will be the difference in the behaviors of the frequency dispersion (Fig. 1a and b) and the dependence on the underlying cooling rate (Fig. 1c) in those two transition regions at around 12 and 28 °C. Because of the different behaviors from the same sample, the difference should not be due to thermal contact or thermal conductivity in the sample. In the following, we discuss the details of the frequency dispersion at the respective peak temperatures of 12 and 28 °C.

4.1. Transition from the intermediate phase to the martensitic phase

The behavior is examined at the peak temperature of 12 °C, and the frequency dispersion of the plots are shown in Fig. 2, as the plots of the real and imaginary parts against frequency (Fig. 2a and b) and in the Cole–Cole plot (Fig. 2c). The Cole–Cole plot shown in Fig. 2c is close to hemicycle and indicates that the frequency dispersion is roughly approximated by the frequency response function of Debye's type, and the plots in Fig. 2a and b shows the systematic shift of the frequency dependence with underlying cooling rate, β: i.e. shorter characteristic time τ with faster β supporting the applicability of the analysis described in the above.

From the frequency dispersion, we evaluated τ by applying the following approximate form of the response function of Debye's type of Eq. (6) for $\omega\tau \gg 1$,

$$\widetilde{\Delta C}'' \simeq -\frac{\bar{F}}{2\pi\beta\tau} \times (\text{period}) \tag{9}$$

where $\bar{F}$ is determined from the peak height of the underlying heat flow, $\dot{\bar{Q}}$, which is shown in Fig. 1a as $-\dot{\bar{Q}}/\beta$. Fig. 3 represents the dependence on the modulation period of the imaginary part, $\widetilde{\Delta C}''$, shown in Fig. 2b. From the slope of the linear fitting, the characteristic time at the respective underlying cooling rates has been determined with Eq. (9).

Fig. 4 represents the dependence on the underlying cooling rate of the characteristic time. The power, x, is close to 1 and this result indicates that the ΔT dependence of the transition rate is exponential: $y = \infty$ in Eqs. (5), (7) and (8). This dependence is consistent with nucleation-controlled transition expected for this transition from the intermediate phase to the martensitic phase. For the further investigation of the nature

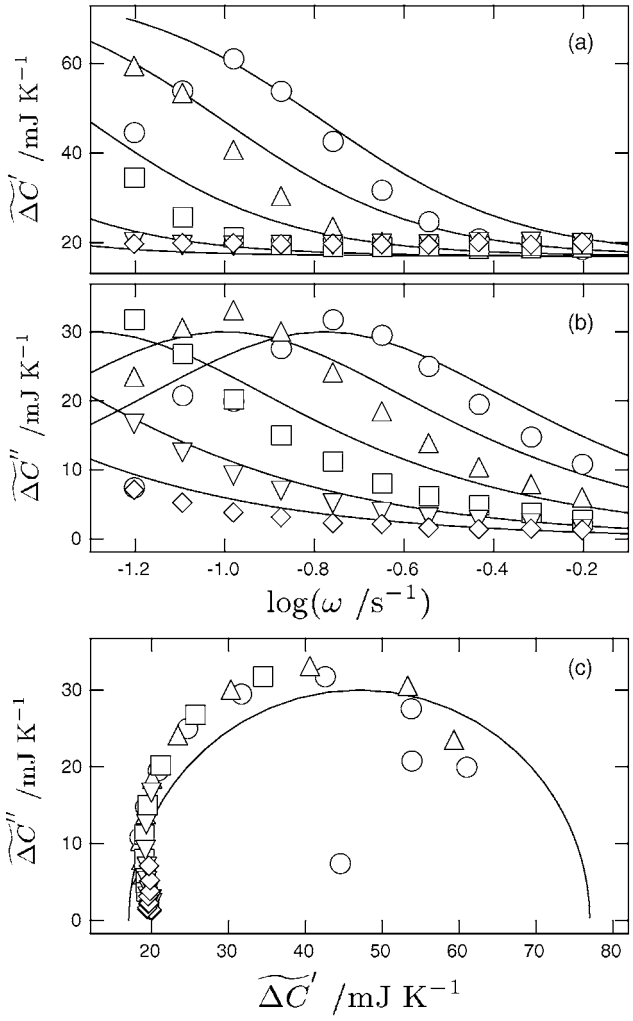

Fig. 2. Dependences on the modulation frequency of (a) the real and (b) the imaginary parts of the effective heat capacity at the peak temperature of 12 °C on cooling at the rates of $-\beta = 3.2$ (○), 1.6 (△), 0.8 (□), 0.4 (▽), and 0.2 K min^{-1} (◊). In (c), Cole–Cole plot of the real and imaginary parts is represented. The solid lines represent the fitting by the frequency response function of Debye's type represented as Eq. (6).

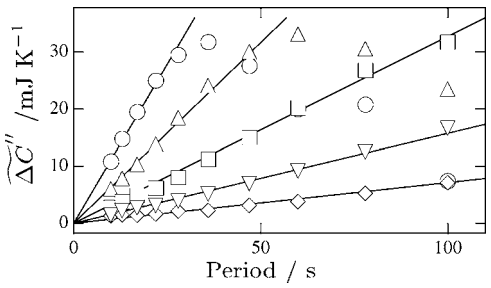

Fig. 3. The dependence on the modulation period of the imaginary part of the effective heat capacity shown in Fig. 2b. The meanings of the symbols are the same as in Fig. 2b.

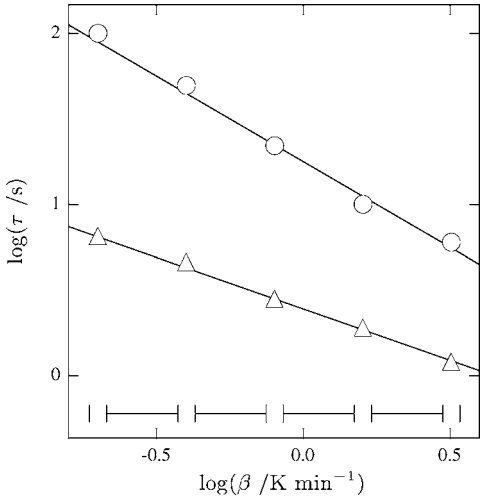

Fig. 4. Logarithmic plots of the characteristic times of transitions at 12 °C (τ: ○) and 28 °C (τ_1: □ and τ_2: △). The characteristic time at 12 °C is determined on the basis of Eq. (9) and the times at 28 °C are in Eq. (10). The slopes of the fitting lines are 1.04 (○) and 0.61 (△).

of this transition, e.g. nucleation barrier, we must determine the transition (peak) temperature [16], which is unavailable with this system because of non-reversible transition behaviors on cooling and heating.

Here, it is needed to mention that the Cole–Cole plot shown in Fig. 2 deviates from the hemicycle expected from Debye's type in a systematic manner. Similar deviation occurred in polymeric systems, and two possible mechanisms of the deviation have been proposed: (1) finite response time of the rate coefficient, R, to the temperature modulation [24] and (2) the modulation of the distribution of transition temperatures caused by the temperature modulation [16]. The second process is related with an annealing effect on the transition temperatures of crystallites, and hence can be confirmed experimentally. Fig. 5 shows the effect of the annealing on the course of linear cooling in the transition region. The shift of the transition temperature to low temperature is clearly seen as the sharp peak only for the transition from the intermediate phase to the martensitic phase after the annealing at 10 °C.

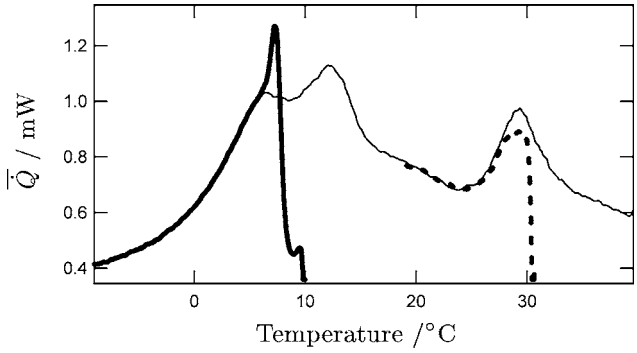

Fig. 5. Heat flow after annealing at 30 (thick broken line) and 10 °C (thick solid line) for 60 min on the way of linear cooling at 1 K min^{-1}. Thin line represents the result without annealing at the same cooling rate.

Therefore, the deviation will be explained by the modulation of the transition temperatures by the periodic temperature modulation.

4.2. Transition from the parent phase to the intermediate phase

The frequency dispersion at the peak temperature of 28 °C is shown in Fig. 6 as the plots similar to Fig. 2. The frequency dependence shown in Fig. 6 is quite different from that of the transition at 12 °C in Fig. 2. The differences are characterized by the systematic decrease of the peak in the imaginary part and flattening of the hemicycle of the Cole–Cole plot with slower underlying cooling rate, as shown in Fig. 6b and c, respectively. In order to explain the systematic change in the frequency dependence for different underlying cooling rate, we think of the superposition of two independent frequency response functions with different dependences of the characteristic times on the underlying cooling rate, as follows,

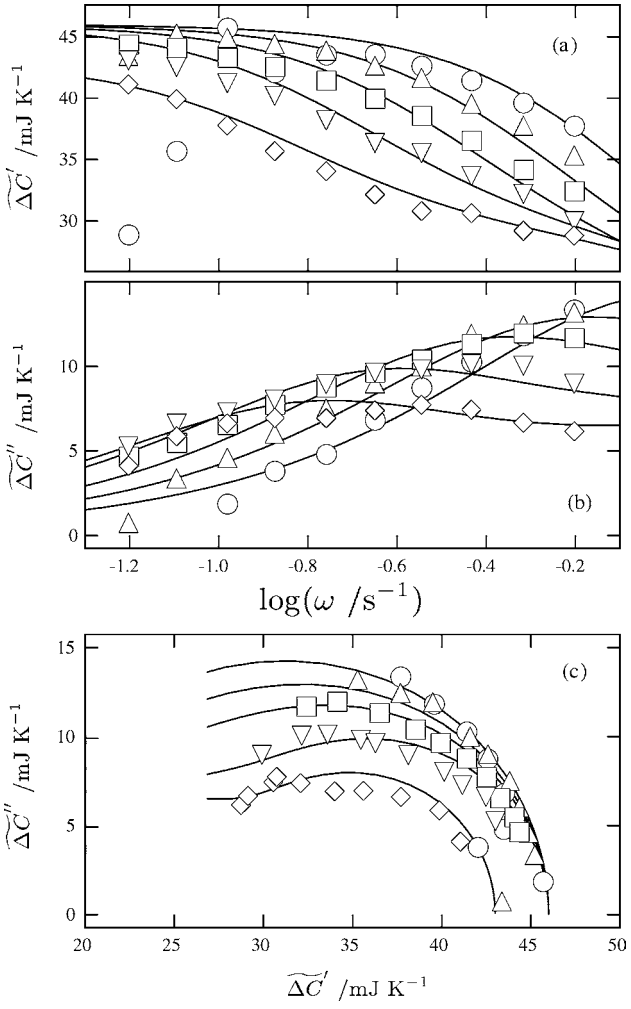

Fig. 6. Dependences on the modulation frequency of (a) the real and (b) the imaginary parts of the effective heat capacity at the peak temperature of 28 °C on cooling at the rates of $-\beta = 3.2$ (○), 1.6 (△), 0.8 (□), 0.4 (▽), and 0.2 K min^{-1} (◇). Cole–Cole plot is shown in (c).

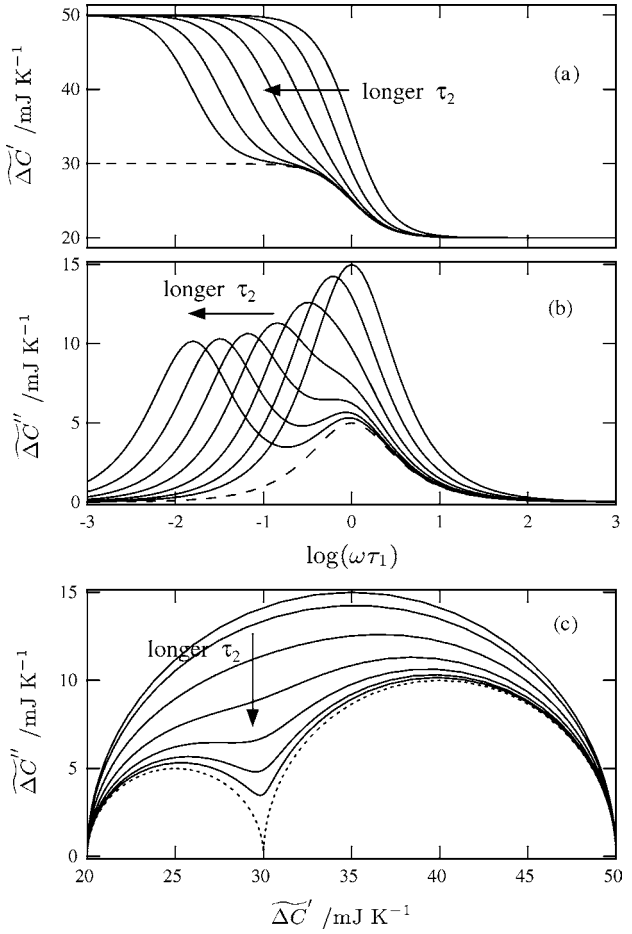

Fig. 7. Plots of the expected dependence on modulation frequency of (a) the real and (b) the imaginary parts of the effective heat capacity on the basis of Eq. (10) with $C_0 = 20$ mJ K^{-1}, $A_1 = 10$ mJ K^{-1}, $A_2 = 20$ mJ K^{-1}, $\tau_1 = 1$ s, and $\tau_2 = 1$, 2, 4, 8, 16, 32, and 64 s. Cole–Cole plot is shown in (c).

$$\widetilde{\Delta C}\, e^{-i\alpha} = C_0 + \frac{A_1}{1 + i\omega\tau_1} + \frac{A_2}{1 + i\omega\tau_2(\beta)} \qquad (10)$$

where C_0, A_1, and A_2 are constants. If only τ_2 is dependent on β, a crossover of the frequency dependence with β is expected as seen in the plots shown in Fig. 7. The fitting curves in Fig. 6 are drawn with the expression of Eq. (10); the best fitting was obtained with τ_1 fixed at 0.6 s (□) and τ_2 (△) shown in Fig. 4.

The power, x, of the β dependence of τ_2 shown in Fig. 4 is close to 0.5 and indicates linear dependence on ΔT of the transition rate: $y = 1$ in Eqs. (5), (7) and (8). This dependence is consistent with the nature of this transition which is almost reversible with negligible nucleation barrier.

In terms of the component with constant characteristic time, τ_1, the modeling of the transition kinetics with Eq. (4) indicates the transition rate being independent of supercooling, i.e. $x = y = 0$ in Eqs. (5), (7) and (8), which should be characteristic of the second-order phase transition. The detailed examination of the transition from the parent phase to

the intermediate phase in $Ti_{50}Ni_{47}Fe_3$ alloy [25,26] has indicated that the transition is composed of two independent transitions occurring successively: transitions from the parent phase to an incommensurate phase and from the incommensurate phase to the commensurate (rhombohedral) phase. The transition to the incommensurate phase is supposed to be second order, and hence the characteristic time, τ_1, may be assigned to this transition. If that is the case, the frequency dispersion with τ_1 and τ_2 means the second-order phase transition from the parent phase to the incommensurate phase and the first-order phase transition from the incommensurate phase to the commensurate phase with negligible nucleation barrier, respectively. In terms of the temperature region of those transitions, with the shorter characteristic time of τ_1 in comparison with τ_2, the frequency dispersion shown in Fig. 1b indicates that the second-order phase transition corresponding to τ_1 can be distinguished as a small peak (thick arrow in Fig. 1b) with weaker frequency dependence within the peak around 28 °C. The appearance of this transition at the higher temperature part of the peak around 28 °C agrees with the order of the phase transitions on cooling: the second-order phase transition from the parent phase to the incommensurate phase and then the first-order phase transition from the incommensurate phase to the commensurate phase.

On the other hand, recent reports suggest that the transition in $Ti_{50}Ni_{48}Al_2$ [27], $Ti_{50}Ni_{48}Fe_2$ [28] and $Ti_{49.3}Ni_{50.7}$ [29] alloys occurs from the parent phase directly to the commensurate phase [27], and the incommensurate phase exists in the parent phase in a wide temperature range [28,29]. If it is the case, the above interpretation of the constant characteristic time, τ_1, cannot be accepted and we need to consider other possibilities. The modeling with Eq. (4) assumes the system composed of small crystallites, and each domain of crystallite is assumed to have a definite transition temperature, while the transition temperature distributes over a wide range for different domains. For the solid–solid transition in the Ti–Ni alloy, we will be able to think of another possibility of continuous distribution of transition temperature in each domain due to complex stress field around the domain considered. In this case (see Appendix A), the power, x, of the β dependence of τ is determined by the ΔT dependence of the propagation velocity, v, of the transition interface in each domain, and the relation is expressed as,

$$v \propto \Delta T^n \tag{11}$$

$$\tau \propto |\beta|^{-1+1/n} \tag{12}$$

Therefore, $x = 0$ of τ_1 indicates linear dependence ($n = 1$) on ΔT of the propagation velocity. This dependence, as well as similar dependence of the rate coefficient indicated by τ_2, will be consistent with the nature of this transition of the first order with negligible nucleation barrier. If it is the case, the present result of the mixed frequency dispersion means the mixture of domains having definite transition temperatures and having the distribution of transition temperature inside the domains.

As shown in Fig. 4, the shortest characteristic time (□) is the constant one and the second one (△) is $\tau_2 \propto \beta^{-0.5}$. Both of them are observed at the transition from the parent phase to the intermediate phase, while the longest characteristic time (○) is with $\tau_1 \propto \beta^{-1}$ observed at the transition from the intermediate phase to the martensitic phase. From their β dependences, it is concluded that the shorter characteristic times are with negligible nucleation barrier, while the longest one is with appreciable nucleation barrier. Therefore, the length of the characteristic times follows the order expected from the barrier height of respective transitions.

Finally, it is noted that the fitting with Eq. (10) shown in Fig. 7 also indicates the decrease in $C_0 + A_1 + A_2$ at lower underlying cooling rate. This change cannot be explained if the strength, A_1 and A_2, are constants. If one of the rate coefficients corresponding to A_1 or A_2 requires finite response time to the temperature modulation, the change in the strength can be expected [24]. If the characteristic time of the response becomes longer with slower underlying cooling rate, β, we can expect smaller strength of A_1 or A_2 for slower β. The meaning of this behavior is not clear.

5. Conclusion

"Periodically modulated driving force" with T-M DSC is applied to the transition kinetics of solid–solid transitions of parent–intermediate phases and intermediate–martensitic phases in Ti_xNi_{100-x}, $x \simeq 50$ at.%. The present results confirm that the frequency dispersion obtained by T-M DSC cannot be due to thermal contact or thermal conductivity in the sample because quite different responses of the kinetics have been observed for the transitions in the same sample with relatively good thermal conductivity.

By the periodically modulated driving force applied with T-M DSC, the nature of the transition kinetics is examined in terms of the response to the modulation in supercooling (temperature) appearing in the dependence of the effective heat capacity of complex quantity on the applied frequency and on the underlying linear cooling rate, β.

Concerned with the transition of intermediate–martensitic phases, the β dependence of the characteristic time of the kinetics, τ, was close to $\tau \propto |\beta|^{-1}$, which indicates an exponential dependence on ΔT of the rate coefficient and hence nucleation controlled kinetics of this transition. This result is consistent with the common understanding of this transition known to be first-order with strong hysteresis.

On the other hand, in the transition region from the parent phase to the intermediate phase, the frequency dependence cannot be expressed by a single dispersion but as a superposition of two different dispersions with τ_1 independent of β and $\tau_2 \propto |\beta|^{-0.5}$. The dependence of τ_2 indicates the rate coefficient in proportion to ΔT and is consistent with the nature of this transition which is supposed to be almost reversible with negligible hysteresis. For the frequency dispersion with τ_1 independent of β, two possibilities have been proposed:

(1) the second-order phase transition or (2) the propagation velocity of the interface in proportion to ΔT with continuous distribution of transition temperature in each domain. The former case corresponds to the successive occurrence of the second-order phase transition from the parent phase to the incommensurate phase and the first-order phase transition from the incommensurate phase to the commensurate phase, which has been proposed by Hwang et al. [25,26]. On the other hand, the second case corresponds to the direct transformation of the first order from the parent phase to the intermediate phase with continuous distribution of transition temperature in each domain [27–29]. Although the distinction between those cases needs further investigations on the details of the transition kinetics, it should be emphasized that the application of T-M DSC enables us to examine those complex behaviors of transformation kinetics.

Acknowledgement

This work was partly supported by a Grant-in-Aid for Scientific Research from Japan Society for the Promotion of Science.

Appendix A

We examine the case of continuous distribution of transition temperature in a one-dimensional single domain with a unit width; the geometry will also model the propagation of the interface of two- or three-dimensional domain if the variation in transition temperature along the interface is small enough and the curvature is small enough.

We assume the propagation velocity of the transition interface, v, dependent on ΔT, as follows,

$$v = \dot{\ell} = a\Delta T^n \tag{A.1}$$

where ℓ represents the position of the interface, and n and a are constants. We consider the transition on cooling and the distribution of transition temperature is assumed to be linear, i.e. $T_{\mathrm{tr}} = T_{\mathrm{tr}}^{\max} - b\ell$, with the highest transition temperature, $T_{\mathrm{tr}}^{\max}$, and a coefficient, b. Then, the above equation is rewritten as,

$$\dot{\ell} = a(T_{\mathrm{tr}}^{\max} - b\ell - T)^n \tag{A.2}$$

When we start the cooling from $T_{\mathrm{tr}}^{\max}$, we have the stationary solution for the steady cooling of the sample temperature, $T = T_{\mathrm{tr}}^{\max} + \beta t$ ($\beta < 0$), as follows,

$$\ell_{\mathrm{st}} = \frac{|\beta|}{b}t - \frac{1}{b}\left(\frac{|\beta|}{ab}\right)^{1/n} \tag{A.3}$$

With a small periodic perturbation applied to the steady cooling of sample temperature, $T = T_{\mathrm{tr}}^{\max} + \beta t + \tilde{T}\,\mathrm{e}^{\mathrm{i}\omega t}$, the response is expressed as,

$$\ell \simeq \ell_{\mathrm{st}} - \frac{\tilde{T}/b}{1 + \mathrm{i}\omega\tau}\,\mathrm{e}^{\mathrm{i}\omega t} \tag{A.4}$$

$$\tau \equiv \frac{|\beta|^{-1+1/n}}{n(ab)^{1/n}} \tag{A.5}$$

Heat flow, F, created by the transition kinetics will be given as,

$$F \equiv F_{\mathrm{st}} + F_T'\tilde{T}\,\mathrm{e}^{\mathrm{i}\omega t} = \dot{\ell}\Delta h \tag{A.6}$$

with the transition enthalpy per unit volume, Δh. The response to the temperature modulation, $F_T'\tilde{T}\,\mathrm{e}^{\mathrm{i}\omega t}$, determines the kinetic component in the effective heat capacity expressed as [6],

$$\widetilde{\Delta C}\,\mathrm{e}^{-\mathrm{i}\alpha} = C_{\mathrm{p}} + \frac{\mathrm{i}}{\omega}F_T' = C_{\mathrm{p}} + \frac{\Delta h/b}{1 + \mathrm{i}\omega\tau} \tag{A.7}$$

References

[1] D.P. Dautovich, G.R. Purdy, Can. Met. Quart. 4 (1965) 129–143.
[2] D.P. Dautovich, Z. Melkvi, G.R. Purdy, G.V. Stager, J. Appl. Phys. 37 (1966) 2513–2514.
[3] S. Miyazaki, C.M. Wayman, Acta Met. 36 (1988) 181–192.
[4] K. Otsuka, X. Ren, Mater. Sci. Eng. A 273 (1999) 89–105.
[5] S. Miyazaki, Shape Memory Alloys in CISM Courses and Lectures, Springer, Wien, 1996, pp. 69–147.
[6] A. Toda, C. Tomita, M. Hikosaka, Y. Saruyama, Polymer 39 (1998) 5093–5104.
[7] P.S. Gill, S.R. Sauerbrunn, M. Reading, J. Therm. Anal. 40 (1993) 931–939.
[8] M. Reading, D. Elliott, V.L. Hill, J. Therm. Anal. 40 (1993) 949–955.
[9] M. Reading, A. Luget, R. Wilson, Thermochim. Acta 238 (1994) 295–307.
[10] B. Wunderlich, Y. Jin, A. Boller, Thermochim. Acta 238 (1994) 277–293.
[11] A. Boller, Y. Jin, B. Wunderlich, J. Therm. Anal. 42 (1994) 307–330.
[12] I. Hatta, Jpn. J. Appl. Phys. 33 (1994) L686–L688.
[13] A. Toda, T. Oda, M. Hikosaka, Y. Saruyama, Thermochim. Acta 293 (1997) 47–64.
[14] A. Toda, C. Tomita, M. Hikosaka, Y. Saruyama, Thermochim. Acta 324 (1998) 95–108.
[15] A. Toda, T. Arita, M. Hikosaka, J. Therm. Anal. Calorim. 60 (2000) 821–827.
[16] A. Toda, Y. Takahashi, T. Arita, M. Hikosaka, T. Furukawa, J. Chem. Phys. 114 (2001) 6896–6905.
[17] Z.G. Wei, R. Sandstrom, Mater. Sci. Eng. A 273–275 (1999) 352–356.
[18] W.A. Brantley, M. Iijima, T.H. Grentzer, Thermochim. Acta 392/393 (2002) 329–337.
[19] I. Hatta, S. Muramatsu, Jpn. J. Appl. Phys. 35 (1996) L858–L860.
[20] A. Toda, T. Arita, C. Tomita, M. Hikosaka, Polymer 41 (2000) 8941–8951.
[21] I. Okazaki, B. Wunderlich, Macromolecules 30 (1997) 1758–1764.
[22] K. Ishikiriyama, B. Wunderlich (Eds.), J. Polym. Sci. B, Polym. Phys. 35 (1997) 1877–1886.
[23] D.N. Abujudom, P.E. Thoma, S. Fariabi, Mater. Sci. Forum 56–58 (1990) 565–570.
[24] A. Toda, Y. Saruyama, Polymer 42 (2001) 4727–4730.
[25] C.M. Hwang, M. Meichle, M.B. Salamon, C.M. Wayman, Philos. Mag. A 47 (1983) 9–30.

[26] C.M. Hwang, M. Meichle, M.B. Salamon, C.M. Wayman, Philos. Mag. A 47 (1983) 31–62.
[27] T. Fukuda, T. Saburi, K. Doi, S. Nenno, Mater. Trans. JIM 33 (1992) 271–277.
[28] T. Tamiya, D. Shindo, Y. Murukami, Y. Bando, K. Otsuka, Mater. Trans. JIM 39 (1998) 714–723.
[29] W. Cai, Y. Murakami, K. Otsuka, Mater. Sci. Eng. A 273–275 (1999) 186–189.